

# Performance Evaluation of Various Smoothed Finite Element Methods with Tetrahedral Elements in Large Deformation Dynamic Analysis

Ryoya Iida<sup>1,a)</sup>, Yuki Onishi<sup>1</sup> and Kenji Amaya<sup>1</sup>

<sup>1</sup> Department of Systems and Control Engineering, Tokyo Institute of Technology, Japan

<sup>a)</sup>Corresponding and Presenting author: iida.r.ad@m.titech.ac.jp

;

## Abstract

It is known that Selective ES/NS-FEM-T4 and F-barES-FEM-T4 show far better results than standard FEM with first-order tetrahedral elements in static analysis. These formulations resolve the pressure oscillation and locking problems in finite element (FE) analysis for nearly incompressible materials without increasing DOF. In this paper, we apply these formulations to modal and dynamic analysis and evaluate the accuracy and stability. Some demonstration analyses confirm these methods can show the as good accuracy in dynamic and modal analysis as in static one. They reveal that the time evolution of total energy of F-barES-FEM-T4 diverge exponentially due to the asymmetric components of the stiffness matrices of this formulation.

**Keywords:** Smoothed finite element method, F-bar method, Large deformation, Pressure oscillation, Locking-free, Modal analysis, Dynamic analysis.

## Introduction

Tetrahedral elements are commonly used in practical FE analyses because arbitrary shapes cannot be meshed into hexahedral elements automatically. Additionally, because intermediate nodes easily pop out in large deformation problems, second or higher-order elements are not preferable[8, 9, 3, 10]. However, T4 elements suffer from pressure oscillation and locking in the FE analysis for nearly incompressible materials. Therefore, high-accuracy FE analysis with T4 elements have been in demand.

Recently, Smoothed Finite Element Method (S-FEM) have been proposed. This technique is known for the high-accuracy FE formulations with T4 elements. Edge-based S-FEM (ES-FEM-T4)[4, 1] has good accuracy in isovolumetric deformation without shear locking. However, it suffers from pressure oscillation and volumetric locking, as well as Standard FEM-T4, in the analysis for nearly incompressible materials[4, 6]. Node-based S-FEM (NS-FEM-T4)[4] has good accuracy in volumetric deformation without locking nor strong pressure oscillation. However, it has spurious low energy modes; therefore, it may cause instability in large strain problems[4].

Considering these features, Selective ES/NS-FEM-T4[4, 5] and F-barES-FEM-T4[7], which combine some classical S-FEMs, have been proposed. In Selective ES/NS-FEM-T4, the hydrostatic part of Cauchy stress tensor is evaluated by using NS-FEM-T4 and the deviatoric part of that is calculated by using ES-FEM-T4. On the other hand, in F-barES-FEM-T4, the isovolumetric part of deformation gradient is derived from that of ES-FEM-T4 and the volumetric part is derived through the multiple smoothing among nodes and elements. It is known that these two methods have good accuracy in static analysis.

In this paper, we evaluate the accuracy and stability of NS-FEM-T4, Selective ES/NS-FEM-T4 and F-barES-FEM-T4 in modal and dynamic analysis. A modal analysis of a multi-material cylinder and a dynamic bending analysis of a cantilever are performed with these formulations.

## Methods

In this section, we describe the way to calculate the nodal internal force of F-barES-FEM-T4. That of the other methods is referred to in papers of Liu[4] and Onishi[4, 5].

### Concept of F-barES-FEM-T4

It is known that NS-FEM-T4 can suppress pressure oscillation to a certain degree in FE analysis for nearly incompressible materials. This implies that the node-based smoothing of the relative volume change  $J$  have the effect of low-pass filter for the pressure distribution. Then, in F-barES-FEM-T4, it is expected that a repetitive node-based smoothing suppresses the pressure oscillation more strongly.

Figure 1 illustrates the outline of F-barES-FEM-T4 in 2D problem (i.e., F-barES-FEM-T3) for simplicity. In F-barES-FEM-T4, the deformation gradient  $\mathbf{F}$  at each edge is divided into the isovolumetric part  $\widetilde{\mathbf{F}}^{\text{iso}}$  and the volumetric part  $\widetilde{J}$ . The isovolumetric part  $\widetilde{\mathbf{F}}^{\text{iso}}$  at each edge is calculated as weighted mean of only the adjacent elements in the same manner as ES-FEM-T4. The volumetric part  $\widetilde{J}$  at each edge is calculated as weighted mean of the relative volumetric changes of some surrounding elements which are defined by cyclic smoothings. The smoothed deformation gradient  $\overline{\mathbf{F}}$  is calculated with  $\widetilde{\mathbf{F}}^{\text{iso}}$  and  $\widetilde{J}$  in the manner of F-bar method[2]. Thus, a good accuracy of ES-FEM-T4 in isovolumetric part and stronger suppression of pressure oscillation than NS-FEM-T4 are expected.

### Cyclic Smoothings

In this section, we describe the way to calculate the deformation gradient of volumetric part  $\widetilde{J}$  with cyclic smoothings.

1. Calculate the relative volume change at each element  $^{\text{Elem}}J$  in the same manner as Standard FEM-T4.
2. Calculate the smoothed relative volume change at each node  $^{\text{Node}}\widetilde{J}$  in the same manner as NS-FEM-T4:

$$^{\text{Node}}\widetilde{J} = \frac{\sum_{k \in \text{Node}_n^{\text{E}} \text{Elem}_k^{\text{E}}} J_k^{\text{Elem}} V_k^{\text{ini}} / 4}{\sum_{k \in \text{Node}_n^{\text{E}} \text{Elem}_k^{\text{E}}} V_k^{\text{ini}} / 4}, \quad (1)$$

where  $^{\text{Elem}}_k V_k^{\text{ini}}$  is the initial volume of element  $k$ ,  $\text{Node}_n^{\text{E}}$  is the set of elements attached to node  $n$ .

3. Calculate the smoothed relative volume change at each element  $^{\text{Elem}}\widetilde{J}$  in the same way as NS-FEM-T4:

$$^{\text{Elem}}\widetilde{J} = \frac{1}{4} \sum_{k \in \text{Elem}_e^{\text{N}}} \text{Node}_k^{\text{E}} \widetilde{J}, \quad (2)$$

where  $\text{Elem}_e^{\text{N}}$  is the set of nodes attached to element  $e$ .

4. Repeat step 2. and 3. as necessary to calculate multi-smoothed relative volumetric change  $^{\text{Elem}}\overline{J}$ . In the second or later evaluation of Eq. (1),  $^{\text{Elem}}\widetilde{J}$  is substituted for  $^{\text{Elem}}J$ .

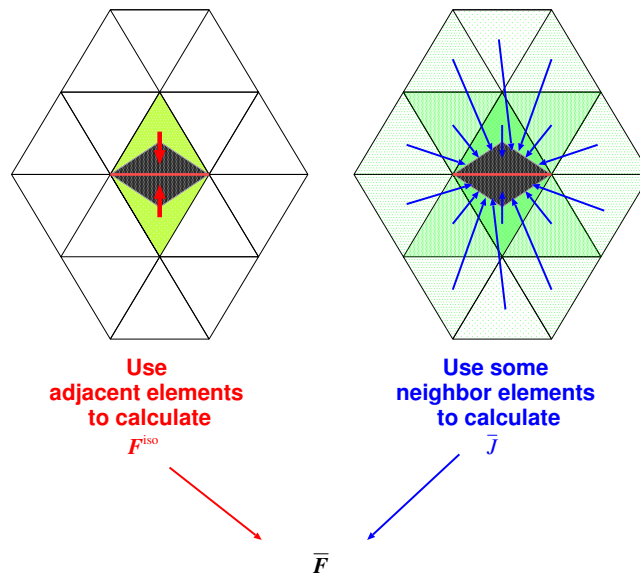


Figure 1. Outline of F-barES-FEM in 2D for simplicity.

5. Calculate the relative volume change at each edge  ${}^{\text{Edge}}\bar{J}$  in the similar way to ES-FEM-T4:

$${}^{\text{Edge}}\bar{J}_h = \frac{\sum_{k \in {}^{\text{Edge}}\mathbb{E}_h} {}^{\text{Elem}}\tilde{J}_k {}^{\text{Elem}}V_k^{\text{ini}}/6}{\sum_{k \in {}^{\text{Edge}}\mathbb{E}_h} {}^{\text{Elem}}V_k^{\text{ini}}/6}, \quad (3)$$

where  ${}^{\text{Edge}}\mathbb{E}_h$  is the set of elements attached to edge  $h$ .

These process means the relative volumetric change  ${}^{\text{Edge}}\bar{J}$  is calculated as the weighted mean of that of the surrounding elements  ${}^{\text{Elem}}J$ .

### Smoothed Deformation Gradient and Nodal Internal Force

We describe the way to calculate the smoothed deformation gradient  ${}^{\text{Edge}}\bar{\mathbf{F}}$  and the nodal internal force. The isovolumetric part  ${}^{\text{Edge}}\tilde{\mathbf{F}}^{\text{iso}}$  is the same with that of ES-FEM-T4  ${}^{\text{Edge}}\mathbf{F}^{\text{iso}}$ :

$${}^{\text{Edge}}\tilde{\mathbf{F}}^{\text{iso}} = {}^{\text{Edge}}\mathbf{F}^{\text{iso}} = \left( \frac{1}{{}^{\text{Edge}}J} \right)^{1/3} {}^{\text{Edge}}\mathbf{F}, \quad (4)$$

where the relative volume change at an edge  ${}^{\text{Edge}}J$  is  $\det({}^{\text{Edge}}\mathbf{F})$ . The volumetric part  ${}^{\text{Edge}}\bar{\mathbf{F}}^{\text{vol}}$  is calculated by using  ${}^{\text{Edge}}\bar{J}$  denoted in previous section:

$${}^{\text{Edge}}\bar{\mathbf{F}}^{\text{vol}} = {}^{\text{Edge}}\bar{J}^{1/3} \mathbf{I}, \quad (5)$$

where  $\mathbf{I}$  is the second-order identity tensor. Smoothed deformation gradient  ${}^{\text{Edge}}\bar{\mathbf{F}}$  is calculated by using these two part in the same manner of F-bar method as follows:

$${}^{\text{Edge}}\bar{\mathbf{F}} = {}^{\text{Edge}}\bar{\mathbf{F}}^{\text{vol}} \cdot {}^{\text{Edge}}\tilde{\mathbf{F}}^{\text{iso}} = \left( \frac{{}^{\text{Edge}}\bar{J}}{{}^{\text{Edge}}J} \right)^{1/3} {}^{\text{Edge}}\mathbf{F}. \quad (6)$$

The smoothed Cauchy stress tensor  $\bar{\mathbf{T}}$  is derived from a material constitutive model and  ${}^{\text{Edge}}\bar{\mathbf{F}}$ .

The nodal internal force vector at an edge  ${}^{\text{Edge}}f^{\text{int}}$  is calculated as follows:

$${}^{\text{Edge}}f_{P:p}^{\text{int}} = \frac{\partial {}^{\text{Edge}}_h \mathbf{D}_{ij}}{\partial \dot{u}_{P:p}} {}^{\text{Edge}}\bar{T}_{ij} {}^{\text{Edge}}V_h, \quad (7)$$

where  $\square_{P,p}$  means the  $p$ -th component of node  $P$ ,  $\dot{u}$  is the nodal velocity and  ${}^{\text{Edge}}_h \mathbf{D}$  is the stretching tensor derived in the same way as ES-FEM-T4.

## Results

### Modal Analysis of Multi-Material Cylinder

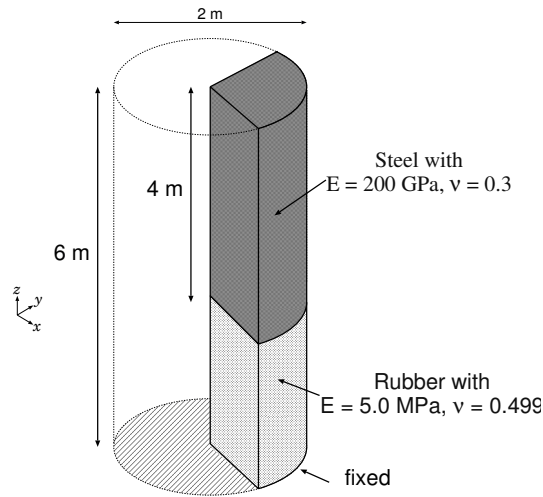
Figure 2 illustrates the outline of the modal analysis of a multi-material cylinder. The analysis domain is a quarter of the cylinder of  $\phi 2 \times 6$  m; its bottom is fixed completely. The upper part of the cylinder is made of steel and the bottom one is made of rubber. The material constitutive model for the analysis domain is linear elastic material. The density, Young's modulus and Poisson's ratio of the steel are  $7800 \text{ kg/m}^3$ ,  $200 \text{ GPa}$  and  $0.3$  respectively, and those of the rubber are  $920 \text{ kg/m}^3$ ,  $5.0 \text{ MPa}$  and  $0.499$ , respectively. The analysis with F-barES-FEM-T4, Selective ES/NS-FEM-T4, NS-FEM-T4 and ABAQUS C3D4 (4-node tetrahedral elements) are performed with unstructured tetrahedral elements of  $0.2 \text{ m}$  global mesh seed size. The analysis with ABAQUS C3D8 (8-node hexahedral elements with selective reduced integration method) of  $0.2 \text{ m}$  global mesh seed size is performed to obtain reference solutions. The number of cyclic smoothings for the steel part is 0 and the one for the rubber part is 1 or 2, in the analysis with F-barES-FEM-T4. The results of F-barES-FEM-T4 are labeled with 'c', which is the number of cyclic smoothings for the rubber part.

Figure 3 shows the comparison of the natural frequencies between various S-FEMs and two ABAQUS elements. The natural frequencies of ABAQUS C3D4 are far higher than reference solution, the result of ABAQUS C3D8, because of

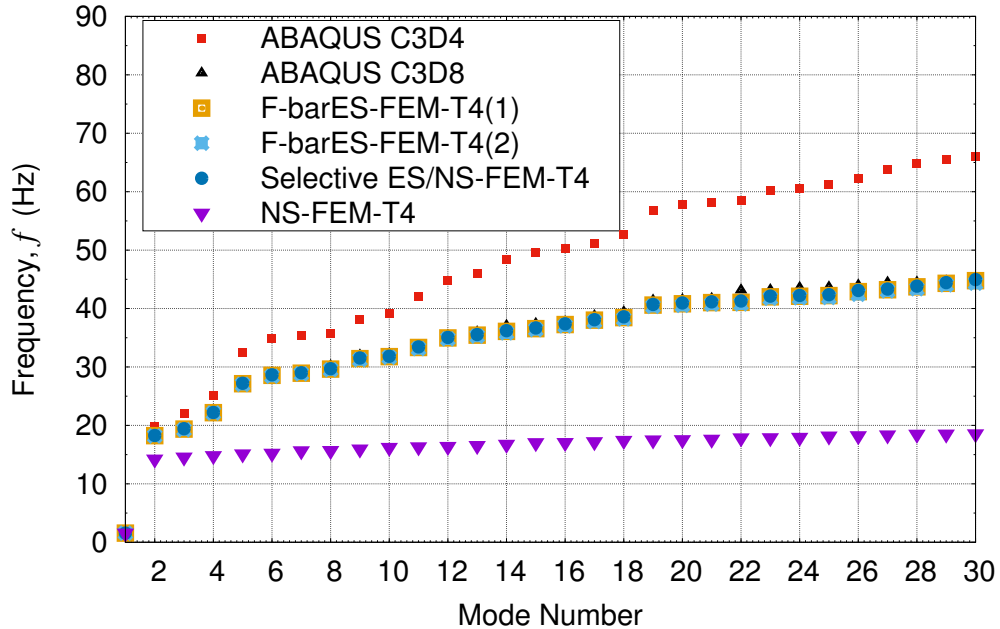
the volumetric locking, and those of NS-FEM-T4 are far lower because of spurious low energy modes. F-barES-FEM-T4 and Selective ES/NS-FEM-T4 show good accuracy of natural frequencies without locking and spurious mode.

Figure 4 and 5 show the mode shapes of the 1st and 11th modes. NS-FEM-T4 shows strange mode shape due to the spurious low energy modes in 11th mode. F-barES-FEM-T4 and Selective ES/NS-FEM-T4 show the similar shapes to ABAQUS C3D8 without locking and spurious modes.

It is known that the stiffness matrix of F-barES-FEM-T4 is asymmetric. The asymmetric property cause complex eigenvalue in modal analysis. Figure 6 shows the distributions of natural frequency of F-barES-FEM-T4(1) and (2).



**Figure 2. Outline of the modal analysis for a multi-material cylinder.**



**Figure 3. Comparison of the natural frequencies vs. mode numbers. The frequencies of ABAQUS C3D4 are higher than those of the others because of the volumetric locking.**

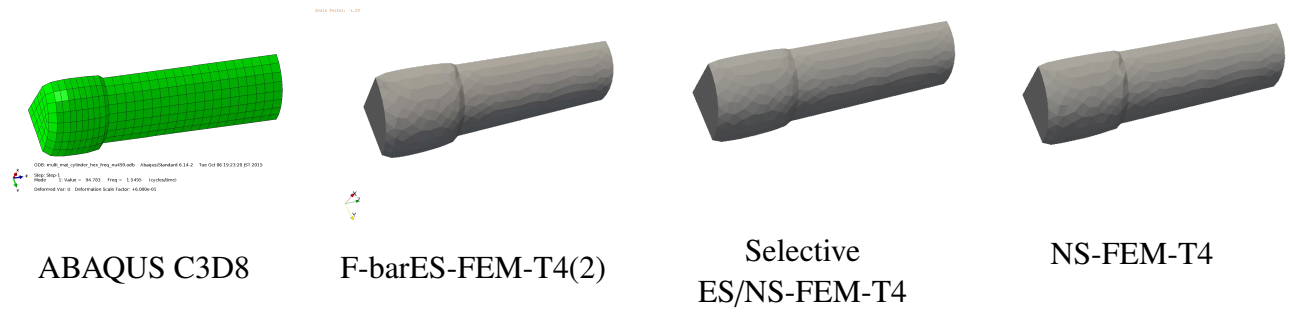


**Figure 4. Mode shapes of the 1st mode.**

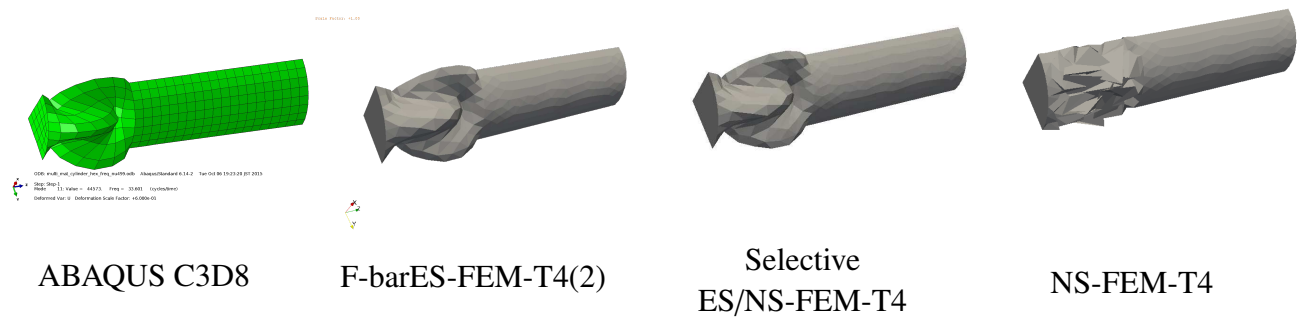


**Figure 5. Mode shapes of the 11th mode.**

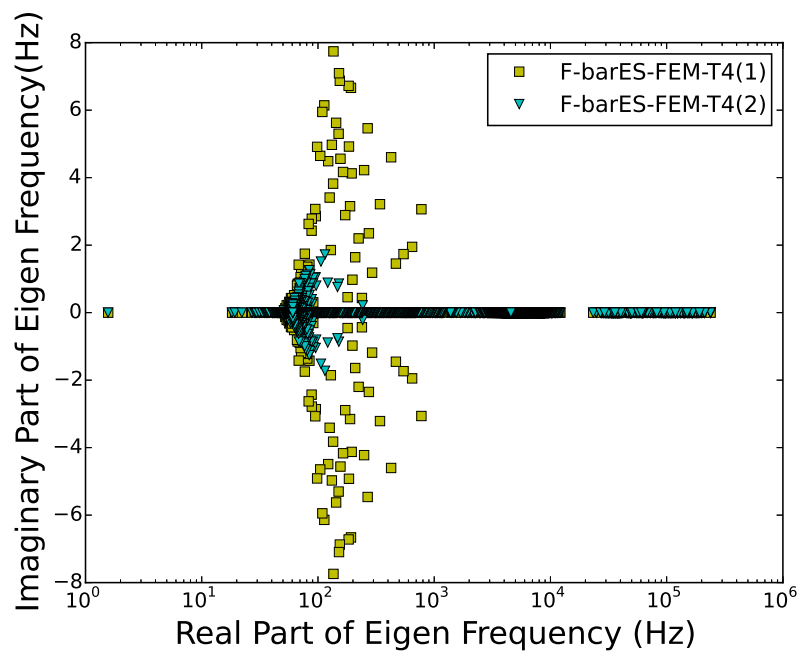


**Figure 6. Distribution of the eigenvalue in the multi material cylinder model with F-barES-FEM-T4(1) and F-barES-FEM-T4(2).**

### Dynamic Bending Analysis of Cantilever

Figure 7 illustrates the outline of the dynamic bending analysis of a cantilever. The analysis domain is a cuboid of  $10 \times 1 \times 1$  m; its left side is perfectly constrained; a uniform initial velocity of 2.0 m/s in  $-z$  direction is applied. The material constitutive model for the analysis domain is Neo-Hookean hyperelastic model. The density, initial Young's modulus and initial Poisson's ratio are  $10000 \text{ kg/m}^3$ , 6.0 MPa and 0.499, respectively. The analysis with F-barES-FEM-T4, Selective ES/NS-FEM-T4, NS-FEM-T4 and ABAQUS/Explicit C3D4 are performed with unstructured tetrahedral elements of 0.2 m global mesh seed size. The analysis with ABAQUS/Explicit C3D8 of 0.2 m global mesh seed size is also performed to obtain a reference solution. The number of cyclic smoothings is 1 to 3, in the analysis with F-barES-FEM-T4. The results of F-barES-FEM-T4 are labeled with 'c', which is the number of cyclic smoothings. In this analysis, the time integration scheme is Velocity Verlet, and the time increment is  $1.0 \times 10^{-4}$  s.

The comparison of the vertical displacements ( $u_z$ ) at one of the corner node ( $\odot$  in Figure 7) is shown in Figure 8. The results of ABAQUS/Explicit C3D4 and NS-FEM-T4 differ from the reference solution due to the locking and spurious low energy modes, respectively. Those of F-barES-FEM-T4s and Selective ES/NS-FEM-T4 agree with the reference; therefore, these formulations have good accuracy without locking in dynamic analysis.

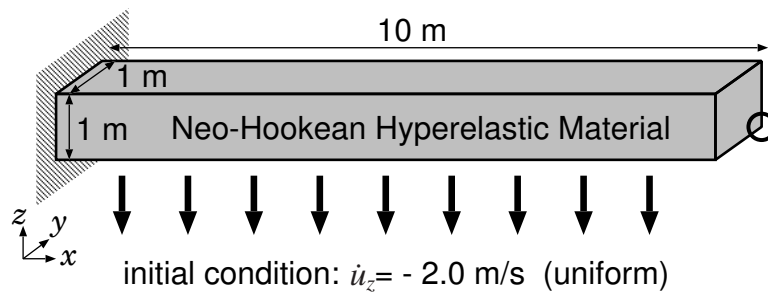
Figure 9 shows the pressure distributions at 1.5 s. In these figures, the value above the range is colored dark red, the one below the range is colored in dark blue and the contour range is  $[-0.223, 0.2813]$  (MPa). The results of NS-FEM-T4, Selective ES/NS-FEM-T4 and F-barES-FEM-T4(1) are different from ABAQUS/Explicit C3D8 at a certain level. Those of F-barES-FEM-T4(2) and (3) agree with the reference; therefore, F-barES-FEM-T4 with sufficient number of cyclic smoothings have good accuracy without pressure oscillation in dynamic analysis.

Figure 10 illustrates the comparison of time-histories of total energy among several formulations. The results of F-barES-FEM-T4s diverge exponentially, and the divergence speeds decrease as the number of cyclic smoothings increasing. This is caused by the imaginary part of the natural frequencies of F-barES-FEM-T4s. As shown in Figure 6, F-barES-FEM-T4 causes complex natural frequencies due to the asymmetric component of the stiffness matrix unlike other methods. When the  $k$ -th natural frequency is a complex number,  $\omega_k = a + ib$  ( $a, b \in \mathbb{R}$ ), time evolution of the  $k$ -th mode shape  $u_k(t)$  is expressed as

$$u_k(t) = \text{Re}\{u_{k0}\} \exp(-i\omega_k t) \quad (8)$$

$$= \text{Re}\{u_{k0}\} \exp(-iat) \exp(bt), \quad (9)$$

where the constant vector  $\{u_{k0}\}$  is defined by initial conditions. If  $b > 0$ ,  $\exp(bt)$  part diverges with time evolution and that is why the results of F-barES-FEM-T4s diverge exponentially. The long time analysis with F-barES-FEM-T4 requires more ingenuity and it is our future work.



**Figure 7. Outline of the dynamic bending analysis of a cantilever. The initial uniform velocity is  $-2.0 \text{ m/s}$  in  $z$  direction.**

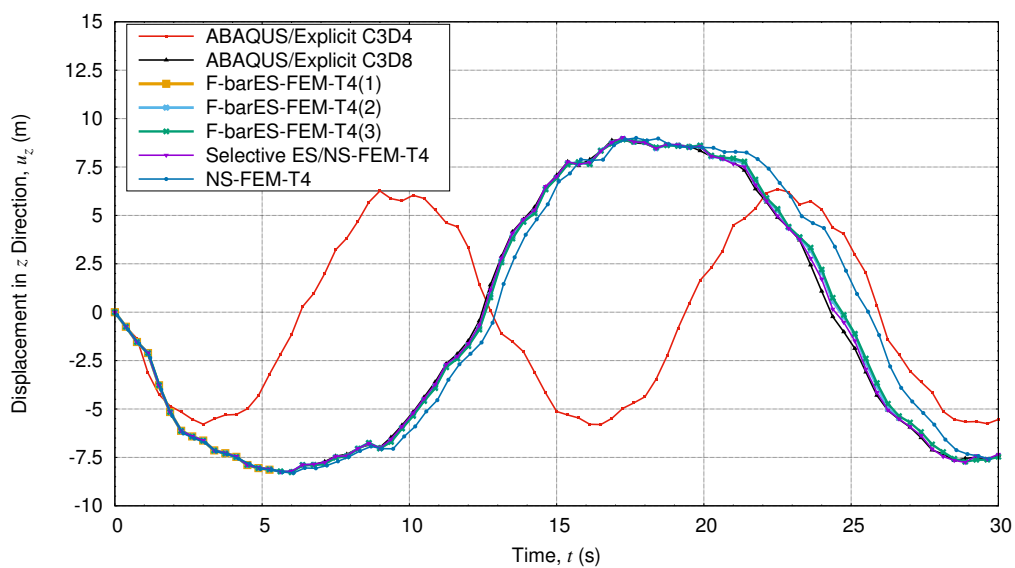


**Figure 8. Comparison of the vertical displacement at the corner vs. time in the cantilever bending analysis.**

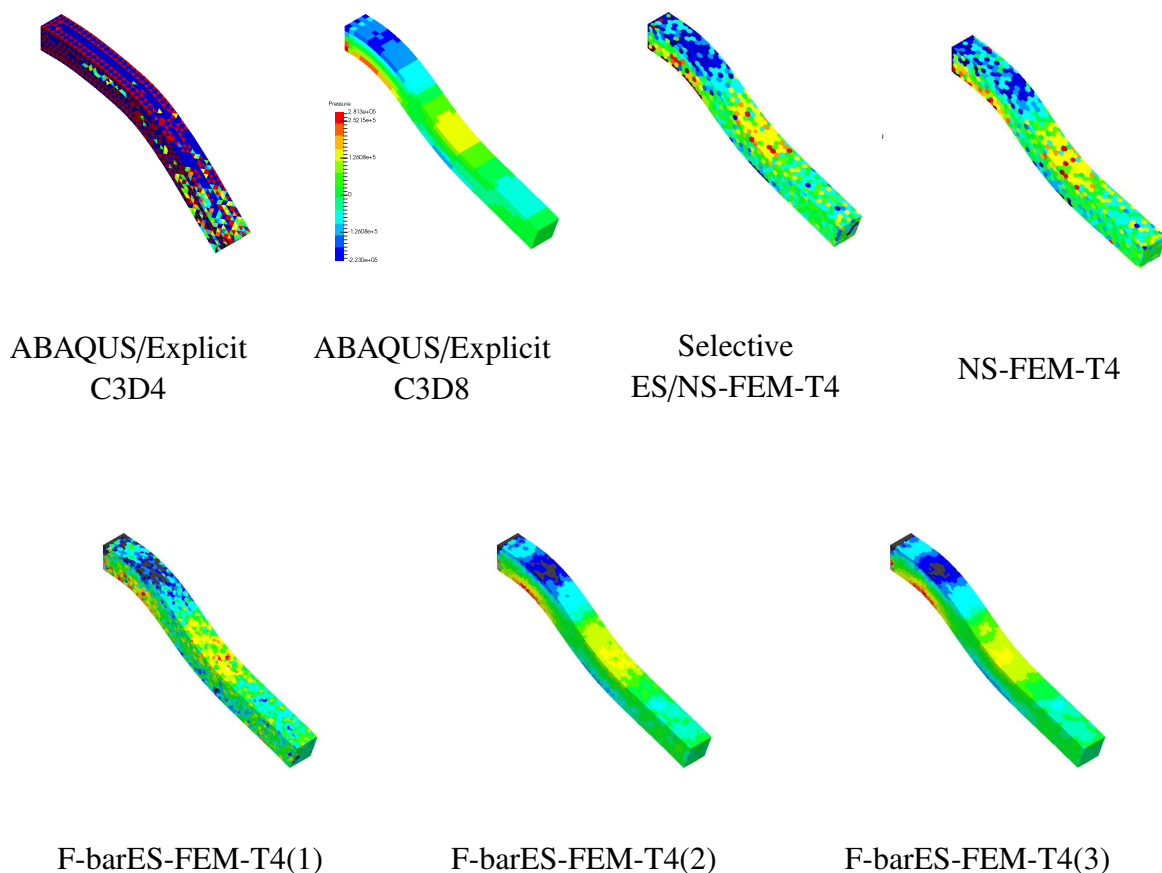


**Figure 9. Deformed shapes and pressure distributions of the dynamic cantilever bending analysis at 1.5 s.**

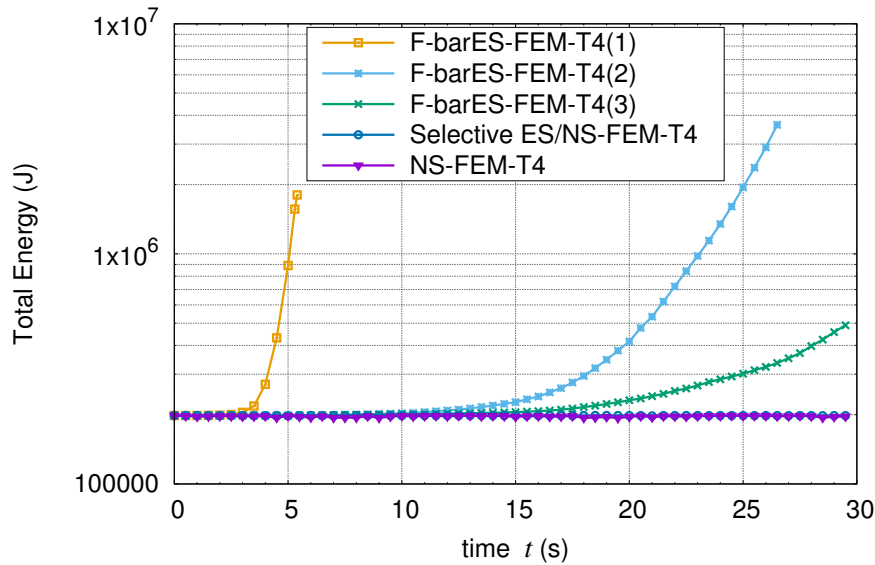


**Figure 10. Comparison of the total energy vs. time for different FEM formulations in the dynamic cantilever bending analysis.**

## Conclusions

We adapted NS-FEM-T4, Selective ES/NS-FEM-T4 and F-barES-FEM-T4 to the modal and dynamic analysis. The features of these formulations are summarized as follows.

- NS-FEM-T4
  - **Modal analysis:** low accuracy due to the spurious low energy modes.
  - **Dynamic analysis:** slightly soft solution in displacement; a little pressure oscillation; no divergence of energy.
- Selective ES/NS-FEM-T4
  - **Modal analysis:** good accuracy without locking nor spurious modes.
  - **Dynamic analysis:** good accuracy in displacement; a little pressure oscillation; no divergence of energy.
- F-barES-FEM-T4
  - **Modal analysis:** good accuracy without locking nor spurious modes.
  - **Dynamic analysis:** good accuracy in displacement; no pressure oscillation with sufficient number of cyclic smoothings; divergence of energy due to the asymmetric property of the stiffness matrix.

The long time analysis with F-barES-FEM-T4 is our future work.

## References

- [1] Cazes, F. and Meschke, G. (2013). An edge-based smoothed finite element method for 3D analysis of solid mechanics problems. *International Journal for Numerical Methods in Engineering*, 94(8):715–739.
- [2] de Souza Neto, E., Peric, D., Dutko, M., and Owen, D. (1996). Design of simple low order finite elements for large strain analysis of nearly incompressible solids. *International Journal of Solids and Structures*, 33(20-22):3277–3296.
- [3] Lee, M. C., Joun, M. S., and Lee, J. K. (2007). Adaptive tetrahedral element generation and refinement to improve the quality of bulk metal forming simulation. *Finite Elements in Analysis and Design*, 43(10):788–802.
- [4] Liu, G. R. and Nguyen-Thoi, T. (2010). *Smoothed Finite Element Methods*. CRC Press, Boca Raton, FL, USA.
- [5] Onishi, Y. and Amaya, K. (2014). A locking-free selective smoothed finite element method using tetrahedral and triangular elements with adaptive mesh rezoning for large deformation problems. *International Journal for Numerical Methods in Engineering*, 99(5):354–371.
- [6] Onishi, Y. and Amaya, K. (2015). Performance evaluation of the selective smoothed finite element methods using tetrahedral elements with deviatoric/hydrostatic split in large deformation analysis. *Theoretical and Applied Mechanics Japan*, 63:55–65.

- [7] Onishi, Y., Iida, R., and Amaya, K. (under review). F-bar aided edge-based smoothed finite element method using tetrahedral elements for finite deformation analysis of nearly incompressible solids. *International Journal for Numerical Methods in Engineering*.
- [8] Son, I.-H. and Im, Y.-T. (2006). Localized remeshing techniques for three-dimensional metal forming simulations with linear tetrahedral elements. *International Journal for Numerical Methods in Engineering*, 67(5):672–696.
- [9] Wan, J., Kocak, S., and Shephard, M. (2005). Automated adaptive 3D forming simulation processes. *Engineering with Computers*, 21(1):47–75.
- [10] Wicke, M., Ritchie, D., Klingner, B. M., Burke, S., Shewchuk, J. R., and O'Brien, J. F. (2010). Dynamic local remeshing for elastoplastic simulation. *ACM Transactions on Graphics*, 29(4):49:1–11. Proceedings of ACM SIGGRAPH 2010, Los Angeles, CA.